Controlling the Ultrafast Dynamics of HD$^+$ by the Carrier-Envelope Phases of an Ultrashort Laser Pulse: A Quasiclassical Dynamics Study

Gaurav Pandey, Diptesh Dey, and Ashwani K. Tiwari*

Indian Institute of Science Education and Research Kolkata, Mohanpur 741246, India

E-mail: ashwani@iiserkol.ac.in

Abstract

A theoretical study on the coupled electron-nuclear dynamics of HD^+ molecular ion under ultrashort, intense laser pulses is performed by employing a well-established quasiclassical model. The influence of laser carrier-envelope phase on various channel ($H+D^+$, $D+H^+$ and H^++D^+) probabilities is investigated at different laser field intensities. The carrier envelope phase is found to govern the dissociation ($H+D^+$ and $D+H^+$) and Coulomb explosion channel (H^++D^+) probabilities. The kinetic energy release distributions of the fragments are also found to be sensitive to the carrier-envelope phase of the laser pulse. Our results are in agreement with the previously reported quantum dynamical studies and experiments.

1. Introduction

One ultimate goal of chemical dynamics is to control the outcome of a chemical reaction to drive it to a desired final state.[1] With the recent advancement in the laser technology, highly intense laser pulses with femtosecond (1 fs = 10^{-15} s) to attosecond (1 as = 10^{-18} s) time duration are readily available and have opened the possibility to achieve this. These ultrashort laser pulses are an ideal tool to probe the electron and nuclear dynamics in real-time.[2,3] Since the magnitude of the optical field of these intense laser pulses are comparable to that of internal coulomb field of molecules, thereby a variety of processes such as above-threshold dissociation(ATD),[4] bond softening(BS),[5] bond hardening,[6] Coulomb explosion(CE)[7] are initiated upon exposure to these intense pulses. In ATD, the molecule absorbs more photons than are required to overcome the bound energy barrier. The additional energy appears as the signature peaks in the kinetic energy release (KER) spectra of the dissociated fragments. BS describes when a molecule's bond 'softens' in the strong laser field and the molecule dissociates. Bond hardening is the process in which an unstable ion or molecule becomes stable upon exposure to ultrashort laser pulse. Dota et al. experimentally observed this bond hardening phenomena for tetramethyl silane.[6] In CE, multiple electrons eject from the

molecule resulting in the formation of a charged molecular cation. Strong coulomb repulsion causes the molecular cation to undergo rapid dissociation. The KER spectra of the dissociated fragments can provide a detailed information about all these processes.

The ultrafast dynamics in atoms and molecules, can be governed by modulating the various laser parameters as controlling knobs, such as, intensity, chirp, pulse duration, and pulse shape etc. With the modern laser technology, it is now possible to generate ultrashort laser pulses consisting of only a few optical cycles. With these laser pulses comprising a few optical cycles, the oscillating carrier electric field plays an important role. The temporal offset between the maximum of the optical cycle and the maximum of the pulse envelope is termed as the carrier-envelope phase (CEP) of the pulse. By a careful choice of laser CEP, it is now possible to control the outcome of the laser-matter interaction on the sub-femtosecond time scales because now the dynamics of the irradiated system is governed by the instantaneous magnitude of the laser pulse and not by the peak intensity of the pulse envelope, which is kept unaltered.[8] Effect of CEP of laser pulses have been demonstrated in several studies such as control of electron emission from atoms,[9,10] electron localization in molecular dissociation,[11,12] and directional fragmentation of molecules.[13] Therefore, CEP of few-cycle pulses plays a crucial role in strong-field control and opens a new prospect to control the ultrafast dynamics with the precision of several hundreds of attoseconds.[14–16]

An accurate description of these strong field processes can be obtained by solving the time-dependent Schrödinger equation taking into account both the electronic and nuclear degrees of freedom. Although much progress has been made in this direction, solving the time-dependent Schrödinger equation for more than two electron system initially bound to the nucleus is still challenging. Some approximate quantum mechanical methods have also been developed in the past decades, such as the multi-configurational time-dependent Hartree-Fock,[17,18] time-dependent density functional theory;[19,20] but their implementation

to polyatomic molecules is still somewhat expensive. Therefore, alternative approaches are necessary to simulate the laser driven atoms and molecules. One alternative method is to use classical mechanics with the quantum nature of the particles to carry out the dynamics. When a molecule is irradiated with a strong laser field with intensity above 10^{14} W/cm^2, the energy levels can be shifted comparable to the field-free energy level differences and therefore, the discrete character of energy levels is washed out. Thus, classical models often work well and is able to interpret several strong field experiments.[21,22] Classical methods also bear several advantages over quantum methods, such as the coupled classical Hamilton's equation of motion being ordinary differential equations instead of partial differential equations as in the time-dependent Schrödinger equation, can be solved easily for a large number of interacting particles. The correlated electron nuclear motion which is very difficult to treat quantum mechanically, can be easily treated by classical mechanics. Since a classical trajectory contains the information of the position and momentum of a particle at any time, therefore, the dynamical processes can be analyzed later in detail by back analysis of the individual trajectories. Specific reaction pathway can be easily identified and the probability of that pathway can be obtained by comparing the trajectories leading to a specific reaction pathway with the total number of trajectories evolved. One such quasiclassical method is the fermionic molecular dynamics (FMD) method. The FMD model was first introduced by Kirschbaum and Wilets et al.[23] and further developed by Cohen.[24] In the FMD model both electrons and nuclei are treated as a point particles; and a non-classical momentum-dependent pseudopotential (V_H) is added to the usual Hamiltonian to stabilize the system.[25] V_H mimics the effect of Heisenberg uncertainty principle which demands that a particle can not be localized in position and momentum simultaneously. FMD model has already been extensively applied to study the laser-induced dynamics of atoms,[22,26] molecules,[27] clusters[28] and atom-ion collision processes.[29–31] Within this quasiclassical method, Huang et al. have investigated the electron momentum distribution from H_2^+ by a circularly polarized laser pulse.[32] By back analysis of the trajectories, they showed that most of the electrons are emitted with a time

lag of hundreds of attoseconds. This delayed emission of the electron was observed in an earlier experiment.[33] Lötstedt et al. applied the FMD model to simulate the dissociation and ionization dynamics of D_3^+ and found an interesting high energy dissociation channel ($D_3^+ \rightarrow D^+ + D^+ + D$) which will be difficult to trace through quantum mechanical simulations using finite-sized grid for wave packet propagation.[34] Quantum dynamical methods can also track these high energy channels, but at the expense of much higher computational cost with increasing grid size. Dey et al. recently applied the FMD model to study the CEP effect on the ionization dynamics of carbon atom.[35] They have observed the angular distribution of ejected electrons to be significantly affected by the CEP of the laser pulse. Experimentally, Paulus et al. also showed that the direction of electron emission from photoionized Ar and Kr atoms can be controlled by varying the laser CEP.[9,36]

In the present work, we have implemented this well-established quasiclassical FMD method to study the influence of CEP of an ultrashort laser pulse on the electronic and nuclear dynamics of HD^+ molecule. We performed full dimensional calculations on HD^+ taking into account the different initial vibrational states and various laser intensities. Since the effect of CEP of ultrashort, intense field on the ultrafast dynamics of HD^+ in presence of competing dynamical processes (dissociation, Coulomb explosion) within the framework of a quasiclassical model is not studied yet, in this article we mainly address the following questions: Is there any CEP effect on the various channel probabilities and nuclear KER distribution for a randomly oriented HD^+ molecule taking into account the full dimension? Is it possible to explain the influence of CEP on the coupled electron-nuclear motion quasiclassically? How the quasiclassical results differ from the quantum mechanical and the experimental results?

The rest of this paper is organized as follows. In Sec.II, the FMD model is briefly described along with the numerical simulation details. Sec.III presents the results and are discussed in details. Sec. IV summarizes and concludes this paper.

2. Theoretical Model and Simulation Details

The field-free Hamiltonian in FMD model for a HD$^+$ ion is given by[32,37] (atomic units are used throughout unless stated otherwise):

$$H = \frac{1}{2}p_e{}^2 + \frac{1}{2m_b}p_b{}^2 + \frac{1}{2m_c}p_c{}^2 - \frac{1}{r_{be}} - \frac{1}{r_{ce}} + \frac{1}{r_{bc}}$$
$$+ \frac{1}{\mu_{be}r_{be}^2}f(r_{be}, p_{be}; \xi_H) + \frac{1}{\mu_{ce}r_{ce}^2}f(r_{ce}, p_{ce}; \xi_D) + \frac{1}{\mu_{oe}r_{bc}^2}f(r_{oe}, p_{oe}; \xi_1) \tag{1}$$

where

$$f(r, p; \xi) = \frac{\xi^2}{4\alpha}\exp\left\{\alpha\left[1 - \left(\frac{rp}{\xi}\right)^4\right]\right\}, \tag{2}$$

The seventh, eighth and ninth terms in the Hamiltonian are the model pseudopotentials. These repulsive pseudopotentials simulate the Heisenberg uncertainty principle and thereby prevents the electron from visiting regions of classical phase space that are forbidden quantum mechanically (if the condition $|r||p| > \xi_H$ is violated). This constraint is approximated by potentials of the form $r_{ij}^{-2}f(r, p; \xi)$, where f is a monotonically decreasing function.[23] For large inter particle distances (r) and momenta (p), the values of these pseudopotentials become very small and therefore they hardly affect the dynamics. These additional potentials improve the ground state energy of the molecular ion. The FMD ground state energy of HD$^+$ ion is -0.6032 a.u., which is in excellent agreement with the quantum mechanical equilibrium ground state Born-Oppenheimer energy of -0.5979 a.u. Whereas, we noted an equilibrium internuclear distance of 2.3214 a.u. compared to the benchmark quantum value of 2.0548 a.u.[38]

The label e stands for electron, o represents the midpoint of the two nucleus, b and c stands for H and D nucleus, respectively. The following abbreviations are used: p_e, p_b and p_c are the momentum of electron, H and D nucleus, respectively. The reduced mass

$\mu_{ij} = (m_i m_j)/(m_i + m_j)$ with $m_o = m_b + m_c$, relative distance $r_{ij} = r_j - r_i$ and the relative momentum $p_{ij} = (m_i p_j - m_j p_i)/(m_i + m_j)$. Here i and j denotes any pair of e, b, c and o. The constant parameters of the model potentials are chosen as $\alpha = 4.0, \xi_H = \xi_D = 0.9428, \xi_1 = 0.90$, following Ref.[32]. The proton mass $m_b = 1836.1527$, deuteron mass $m_c = 3670.4830$ and electron mass $m_e = 1$ are used.

The dynamics of the system is followed by numerically solving the coupled Hamilton's equations of motion

$$\frac{d\boldsymbol{r_i}}{dt} = \frac{\partial H}{\partial \boldsymbol{p_i}}, \qquad\qquad \frac{d\boldsymbol{p_i}}{dt} = -\frac{\partial H}{\partial \boldsymbol{r_i}} + Z\boldsymbol{E}(t, r_i)$$

$$\frac{d\boldsymbol{r_e}}{dt} = \frac{\partial H}{\partial \boldsymbol{p_e}}, \qquad\qquad \frac{d\boldsymbol{p_e}}{dt} = -\frac{\partial H}{\partial \boldsymbol{r_e}} - \boldsymbol{E}(t, r_i)$$

(3)

for nuclear charge Z, in the presence of the laser electric field, $\mathbf{E(t)}$ given by

$$E(t) = \hat{x} E_0 e^{-2\ln 2(t-t_0)^2/\tau^2} \, cos(\omega_0 (t - t_0) + \phi) \tag{4}$$

with the laser field strength E_0, angular frequency ω_0, laser pulse duration τ and the CEP of the pulse ϕ. The laser pulse is assumed to be x-polarized. The carrier wavelength was chosen to be 790 nm ($\omega = 0.058$) with a pulse width (FWHM) of 7.1 fs.[39] The dc component of the laser pulse is negligibly small ($< 10^{-8}$ relative to E_0) for all CEP values.

In FMD model, the Hamiltonian defines the total energy of the system which depends on the position and momentum of the particles. Ground state energy of the system is obtained by minimizing the system Hamiltonian with respect to the position and momentum of all the particles. With an initial guess of the position and momentum of the particles, we minimized the Hamiltonian following the downhill simplex method[40] to obtain the exact ground state configuration of the molecular ion. The minimization algorithm was repeated several times with different initial positions and momenta to ensure the attainment of the global minima.

The minimized position and momentum of the particles and the ground state energy of the molecular ion were found to be in a good agreement with earlier reported results.[41] For instance, we obtained a ground state configuration corresponding to the initial optimized geometry for the position coordinates of the H and D nuclei at (1.1607, 0, 0) and (-1.1607, 0, 0), respectively, with X-axis as the initial molecular axis. Field free trajectories were then run with this optimized geometry to ensure the stability of the ground state molecular ion against pre-dissociation and auto-ionization. The simulation mainly consists of three steps: Sampling of the initial conditions, temporal evolution in the presence of laser light, and identification of the final state. For sampling of the initial configurational space, we applied the following procedure.[34] Since the system is stationary, we first imparted an extra vibrational energy (e.g., zero-point energy to reach $v = 0$ state) to the model ion. Then, one field-free trajectory is runned with the initial vibrational state energy for the optimized geometry by ensuring that the energy and the total angular momentum of the ion are conserved. We then choose the position and momentum of the particles at any instant of time along the field free trajectory (to be specific, we choose 100 random points) and applied random rotation matrices to generate an ensemble of the randomly oriented molecules. On each and every point, we applied the random rotation matrices 120 times. Since, the FMD Hamiltonian is invariant with respect to overall rotation, $H(\boldsymbol{r}_e, \boldsymbol{p}_e, \boldsymbol{r}_b, \boldsymbol{p}_b, \boldsymbol{r}_c, \boldsymbol{p}_c) = H(\boldsymbol{\Omega}_1\boldsymbol{r}_e, \boldsymbol{\Omega}_1\boldsymbol{r}_b, \boldsymbol{\Omega}_1\boldsymbol{r}_c, \boldsymbol{\Omega}_2\boldsymbol{p}_e, \boldsymbol{\Omega}_2p_b, \boldsymbol{\Omega}_2\boldsymbol{p}_c)$, where Ω_1 and Ω_2 are two sets of rotation matrices, it does not alter the energy of the system but simply rotates the entire molecule with a random angle with respect to the internuclear axis (X-axis). After rotation, the new coordinates act as the initial condition for the trajectories in the presence of laser field. Thereby, sampling of the initial conditions are done with the random rotation matrices. In this way, we obtained an initial ensemble of 12000 randomly oriented molecules with the same initial energy but different positions and momenta. The laser polarization vector (along X-axis) remains unaltered for every run. Although, the angle between molecular axis and laser polarization vector is not explicitly defined in the Hamiltonian, it can be obtained with the knowledge of the new rotated coordinates. Time-

evolution of the system was then performed by integrating the Hamilton's equations of motion using an adaptive fifth-order Runge-Kutta solver. The total simulation time for each trajectory was 2000 a.u., which is sufficient for the identification of the final state. The error bars in the plots represent the sampling errors calculated by[34]

$$\sigma_j = \sqrt{\frac{n_j(n_{tot} - n_j)}{n_{tot}^3}}, \tag{5}$$

where n_j is the number of trajectories in the jth channel and n_{tot} is the total number of trajectories.

3. Results and Discussion

3.1. Temporal Evolution of the Dynamical Channels

The different dynamical channels are defined as follows:

$$HD^+ + n\hbar\omega \rightarrow HD^+ \ \text{(Survival)} \ r_{bc} < 9.5, \ \epsilon_i < 0$$

$$HD^+ + n\hbar\omega \rightarrow \begin{cases} H + D^+ \ \text{(Dissociation-1)} \ r_{bc} > 9.5, \ \epsilon_i < 0, \ r_{be} < r_{ce} \\ D + H^+ \ \text{(Dissociation-2)} \ r_{bc} > 9.5, \ \epsilon_i < 0, \ r_{be} > r_{ce} \\ H^+ + D^+ + e \ \text{(Coulomb explosion)} \ r_{bc} > 9.5, \ \epsilon_i > 0 \end{cases}$$

$$HD^+ + n\hbar\omega \rightarrow HD^{2+} + e \ \text{(Ionization)} \ r_{bc} < 9.5, \ \epsilon_i > 0.$$

At the end of the simulation, the four dynamical channels, namely, survival ($HD^+ + n\hbar\omega \rightarrow HD^+$), dissociation ($HD^+ + n\hbar\omega \rightarrow H + D^+$ and $H^+ + D$) and Coulomb explosion ($HD^+ + n\hbar\omega \rightarrow H^+ + D^+ + e$) are possible. At the final time, the ionization channel ($HD^+ + n\hbar\omega \rightarrow HD^{2+} + e$) will not be observed because HD^{2+} ion will eventually explode and lead to Coulomb explosion. The bond was assumed to be dissociated when the internuclear distance r_{bc} becomes greater than a cut-off value of 9.5 a.u.[42] The molecular ion is considered to be ionized when the

9

electron energy ϵ_i becomes greater than zero. The electron energy ϵ_i consists of the kinetic energy of the electron, potential energy of the electron-nucleus attraction and the auxiliary potential. To simulate a real experimental situation of randomly oriented molecules in the gas phase, the initial angle between the molecular axis and the laser polarization axis was selected randomly. 12×10^3 trajectories were run to calculate the probabilities and the convergence of the probability values were ensured up to 4 digits from decimal. It is worth pointing out that the processes are occurring in the multiphoton regime and the binding energy of HD$^+$ molecule defined as the least energy required to produce a free electron and two nuclei, in the presence of the field, all infinitely far from each other is calculated to be 0.6032 a.u.
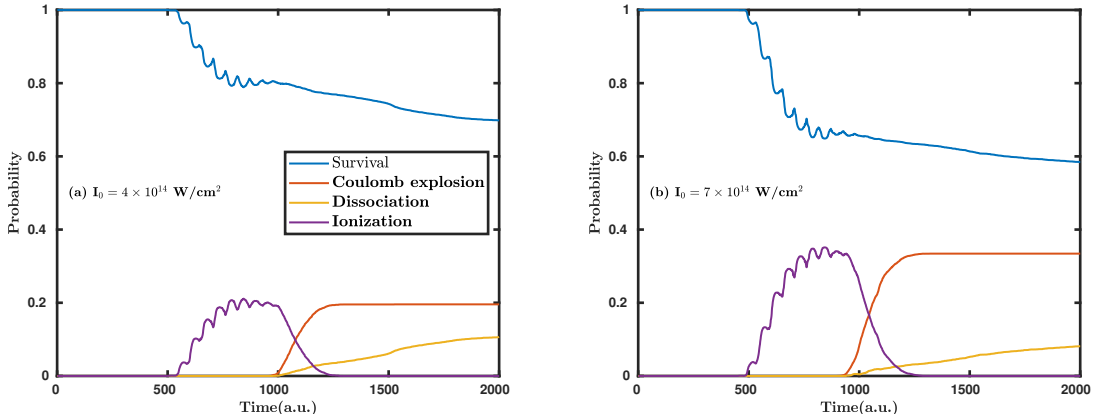

Figure 1: Time evolution of the probabilities of survival, Coulomb explosion, dissociation and ionization for the $v = 0$ state of HD$^+$ molecular ion in the presence of 7.1 fs laser field of 790 nm wavelength.

Fig.1a and Fig.1b show the temporal evolution of various channel probabilities of HD$^+$ ($v = 0$) molecular ion at laser intensities of 4×10^{14} W/cm^2 and 7×10^{14} W/cm^2, respectively. We have ensured the convergence of our results with respect to the total propagation time. Overall, Fig.1 indicates that the ionization channel is first turned on, reaches a maximum value, and then rapidly decreases. This phenomena can be explained in the following way. As the molecular ion absorbs energy from the laser pulse, it ionizes to form HD^{2+}. During this short period of time, the nuclei do not have enough time to get separated. When the ionization is at its peak value, the two ionic cores explode rapidly due to Coulomb repulsion,

10

and at the same time, the Coulomb explosion channel starts to increase with time and reaches the same peak value as that of the ionization channel. Finally, the ionization channel completely disappears. At the maxima of the ionization channel, the dissociation channel also appears along with the Coulomb explosion channel. Two types of mechanisms are possible for the dissociation channel. First, the direct dissociation where a molecule absorbs enough energy to reach the dissociation limit (H+D$^+$ or D+H$^+$). Second, the electron gets ionized at first, and then after a certain time delay, it can get recaptured by either of the ionic cores. These two distinct dissociation mechanisms can be distinguished by the KER spectra of the fragments, which we will discuss later. The qualitative behavior of the channels' temporal evolution is the same for both the laser intensities (as indicated in Fig.1 (a)and (b)), but at a higher laser intensity, the ionization channels' peak rises, which results in the higher probability of the Coulomb explosion channel at the final time.

3.2. Initial Vibrational State and Intensity Dependence

We have studied the effect of initial vibrational states and laser pulse intensities on the dynamical channel probabilities and also compared our quasiclassical results with the quantum mechanical results of Ref.[39] Calculations were performed on the $v = 0, 3, 6$ and 9 initial vibrational states of HD$^+$ molecular ion and laser peak intensity of 1×10^{14}, 2×10^{14}, 4×10^{14} and 7×10^{14} W/cm^2 were chosen. Laser pulse CEP value was taken to be zero. Fig.2(a)-(d) shows the probabilities of survival, dissociation, and Coulomb explosion as a function of the vibrational states of randomly oriented HD$^+$ molecule, at different laser intensities. We have considered four initial vibrational states from $v = 0$ to $v = 9$ because we are mainly interested to investigate the vibrational states which have a sufficient energy gap. Fig.2 clearly indicates this initial vibrational state dependency on the various channels by simply considering four states up to $v = 9$ having significant energy gap. Since 12×10^3 trajectories were run at each initial vibrational state and at each laser intensity, we aimed to obtain maximum physical insight at the expense of minimum computational resources. The total
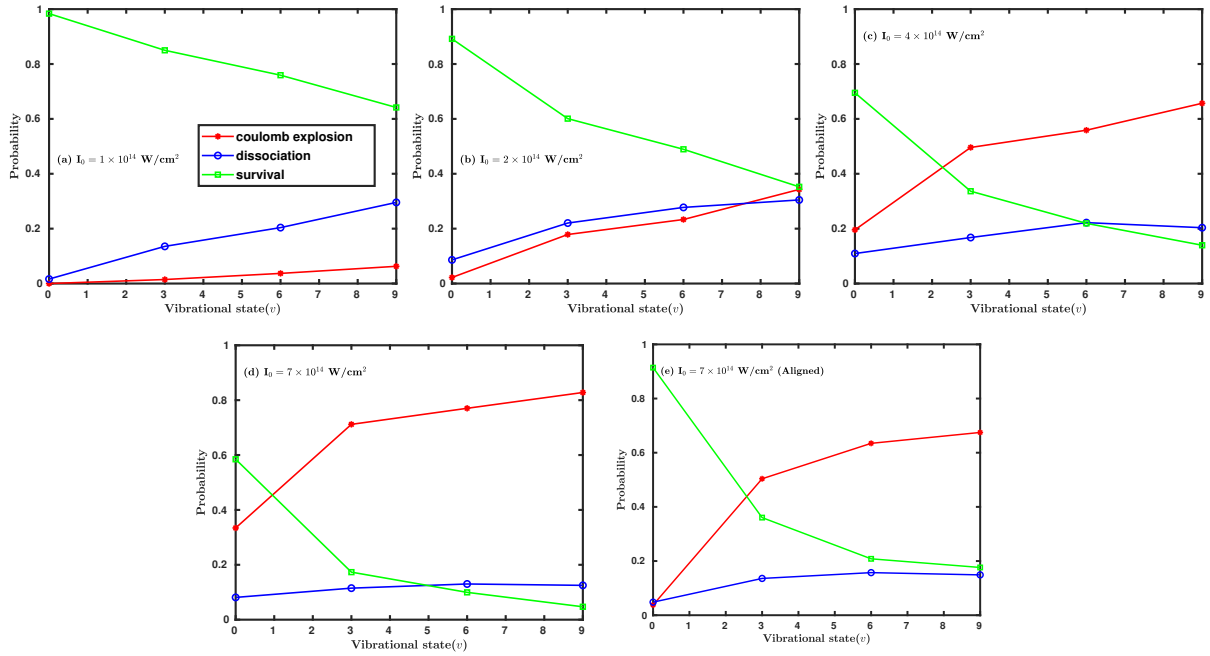
Figure 2: Vibrational state dependence of the probabilities of survival, dissociation and Coulomb explosion of HD$^+$ molecular ion in presence of 7.1 fs laser field of 790 nm wavelength at different intensities, considering a randomly oriented sample (Panels (a)-(d)) and an aligned molecule (Panel (e)) with respect to the laser polarization axis. Laser pulse CEP value was taken to be zero. The statistical error bars are smaller than the symbol size.

dissociation probability shown in Fig.2 consists of the probability of both the pathways, H+D$^+$ and D+H$^+$. It is clear from Fig.2 that the total dissociation and Coulomb explosion channels are strongly dependent on the initial vibrational state and the intensity of the laser pulse. For instance, at a low intensity of 1×10^{14} W/cm^2, shown in Fig.2a, both the dissociation and Coulomb explosion channels increase with increasing the initial vibrational state. However, the dissociation probability is higher than the Coulomb explosion probability for all the initial vibrational states at low intensity. As the intensity of the laser pulse increases, the Coulomb explosion channel starts to dominate. When the intensity reaches the value of 4×10^{14} W/cm^2, for all the initial vibrational states, the Coulomb explosion channel dominates over the dissociation. Quantum mechanically, this trend in dissociation yield (HD$^+$ + $n\hbar\omega \rightarrow$ H+D$^+$ and H$^+$+D) can be explained by adiabatic Floquet potential analysis in terms of bond softening and above-threshold dissociation. Whereas, the Coulomb explosion fragmentation channel can be explained by the charge-resonance enhanced ionization (CREI) model.[43] The total probabilities calculated by the quasiclassical FMD model are qualitatively in agreement with the quantum mechanical results. For the vibrational ground state, quantum calculations showed a significant Coulomb explosion probability at an intensity of 7×10^{14} W/cm^2. Whereas, in our calculation it is observed at 4×10^{14} W/cm^2 intensity. For $v = 3$ state, quantum calculations showed a significant Coulomb explosion channel to start at 4×10^{14} W/cm^2 intensity, whereas, we noted the same at 2×10^{14} W/cm^2 intensity. Quantum calculations reported the onset of the dissociation channel at 4×10^{14} W/cm^2 intensity for $v = 0$ state, in contrast to the same at 2×10^{14} W/cm^2 intensity obtained in our computations. Therefore, for lower vibrational states ($v = 0, 3$), the dissociation and Coulomb explosion channels start at lower intensities in FMD calculations as compared to quantum mechanical calculations. But, for higher vibrational state ($v = 6, 9$), both dissociation and Coulomb explosion channels are consistent with the quantum mechanical results. Fig.2(e) shows the dynamical channel probabilities for the molecule aligned with the laser polarization axis at 7×10^{14} W/cm^2 intensity and it can be directly compared with Fig.2

of Ref.[39]. By aligned molecules we actually meant a perfectly aligned initial orientation of the internuclear axis along the polarization vector of the radiation field. Experimentally this can be difficult to achieve, but theoretically it can be realized. For higher vibrational states ($v = 3, 6, 9$), Coulomb explosion and dissociation channels show similar behavior as the quantum mechanical results. Quantitatively, for instance, the quasiclassical Coulomb explosion and dissociation probabilities for v=6 are 0.6346 and 0.1572, respectively, whereas in the quantum calculation, these are ~ 0.7598 and ~ 0.1459, respectively. Therefore, for higher vibrational states our results for the aligned molecule are in good agreement with the quantum mechanical results. However, there is a noticeable difference between the two for the ground vibrational state. For $v = 0$ state, we noted nearly equal probability for both dissociation (0.0482) and Coulomb explosion (0.0377) channels, whereas, quantum mechanically a much higher Coulomb explosion channel probability (0.4865) is observed than the dissociation channel probability (0.2410). The main difference between the quantum and quasiclassical results arise for the lower vibrational states. We can thus conclude from the quasiclassical FMD model that the discrete character of the low-lying vibrational states is poorly described since FMD allows a continuum of such states to exist. Although, with a Franck-Condon averaging of initial vibrational states a quantitative agreement with the quantum mechanical results can be achieved.

To obtain a further understanding of the competition between dissociation and Coulomb explosion channels, we report the CEP averaged dissociation and Coulomb explosion yields from the initial ground vibrational state of HD^+ in Fig.3. From Fig.3, it is clear that up to about 3×10^{14} W/cm^2 intensity the dissociation channel dominates over Coulomb explosion. Same trend have been observed with the Franck-Condon (FC) averaging of the initial vibrational states by quantum mechanical calculations. Quasiclassically, the maximum total dissociation probability from $v = 0$ state is found at 4×10^{14} W/cm^2 with a value of 0.10, whereas, quantum mechanically FC averaged total dissociation probability is about
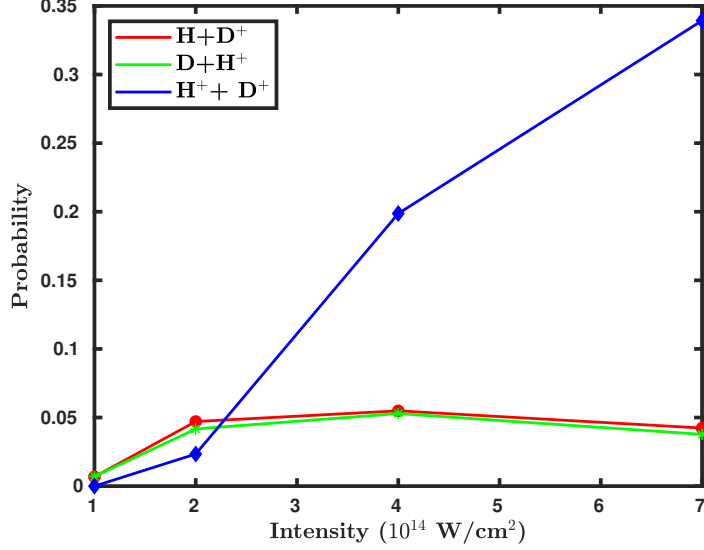
Figure 3: Intensity dependence of the CEP averaged probabilities of the dissociation and Coulomb explosion channels from $v = 0$ state of HD^+ ion. The statistical error bars are smaller than the symbol size.

0.27 at the same intensity. In our quasiclassical calculation, maximum Coulomb explosion probability is 0.34, whereas, previously reported quantum mechanical Coulomb explosion probability is about 0.45 at the intensity 7×10^{14} W/cm^2. It is important to point out from Fig.3 that if the CEP of the pulse is not fixed, then the molecules have an equal probability of dissociating in $H+D^+$ and $D+H^+$.

3.3. Carrier-Envelope Phase Dependence on Different Channel Probabilities

Here we examined the CEP effect on the two dissociation channels $H+D^+$ and $D+H^+$ and on the Coulomb explosion channel (H^++D^+). We performed the calculations at nine different values of CEP ranging from 0 to 2π at a different values of laser intensity. Same laser pulse parameters were taken as in the calculation of total channel probabilities. The dissociation channel probability of HD^+ ion at different values of CEP are shown in Fig.4. From Fig.4, it is clear that both the dissociation channels are dependent on the CEP of
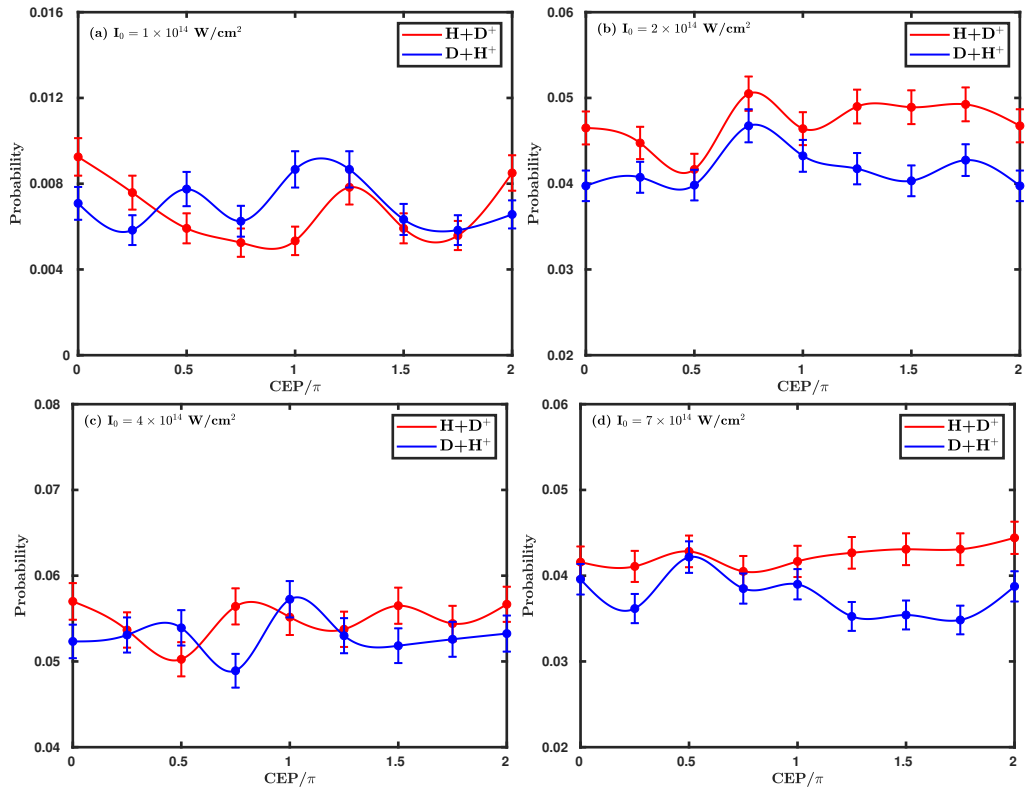
Figure 4: CEP dependence on the dissociation channels of HD$^+$ ion under 7.1 fs (790 nm) laser pulse from the $v = 0$ state. Statistical errors bars are included (see Eq. (5) for details).

the laser pulse. With an intensity of 1×10^{14} W/cm^2 , the H+D$^+$ channel is maximum at $\phi = 0$ and minimum at $\phi = \pi$. Whereas, the D+H$^+$ channel is minimum at $\phi = 0.25\pi$ and maximum at $\phi = \pi$. The maximum difference between the two dissociation channels is found at the CEP value of $\phi = \pi$. At $\phi = 0$, H+D$^+$ channel probability is higher than D+H$^+$ channel, but at $\phi = \pi$ these channel probabilities get reversed and further retained the same behavior at CEP = 2π. Fig. 4 also depicts that the CEP effect also depends on the intensity of the laser pulse. For 2×10^{14}, 4×10^{14} and 7×10^{14} W/cm^2 intensities, the maximum difference between the two dissociation pathways are found at CEP $= 1.5\pi, 0.75\pi$ and 1.75π respectively. By a careful choice of the CEP and the intensity, one of the dissociation channel can be made dominant over the another, which is not possible when the CEP of the pulse is averaged out (Fig.3). The effect of CEP on the branching asymmetry of H+D$^+$ and D+H$^+$ channels can be understood by following the electron dynamics of the dissociating HD$^+$ molecule. For small internuclear separation, the intramolecular potential barrier is low, and the electron can freely move between the two nuclei. As the internuclear separation increases, the potential barrier between the two nuclei also increases, and the electron gets eventually trapped on either of the nuclear cores. Since, the intramolecular motion of the electron is controlled by the laser CEP (instantaneous magnitude of the pulse) rather than the intensity profile, the rapid directional motion of the electron is governed by the CEP.[44] Quasiclassically, the observed CEP effect on the dissociation channels in Fig. 4 is very small and quite different from the quantum mechanical results. One possible reason for the origin of this difference is due to the orientation of the molecule; previously, an oriented HD$^+$ molecule was considered. Rathje et al. experimentally observed the CEP effect on H$_2^+$ aligned $\sim 25°$ with respect to the laser polarization.[45] In our calculations we used randomly oriented molecule which might decrease the CEP effect.[46] A second possibility for the disagreement with the quantum-mechanical results is the poor description of the discrete character of the initial vibrational states in this quasiclassical FMD method. This is a limitation of the FMD model since it allows a continuum of such states and the CEP effect is dependent on

the initial vibrational state of the molecule and on moving to the higher vibrational states, the effect of CEP decreases. A third possibility is due to the limitation of any classical model, where if the pulse length is very short, then the uncertainty principle will come into play. Following the relation, $\Delta E \geq 2\pi/t_{pulse}$, if the pulse length t_{pulse} is very short, a broadening of the energy levels ΔE will occur, ultimately leading to the overlapping of states.

At higher laser pulse intensities, CEP effect is observed on the Coulomb explosion channel $(H^+ + D^+)$ and is shown in Fig.5. Coulomb explosion channel shows oscillatory behavior
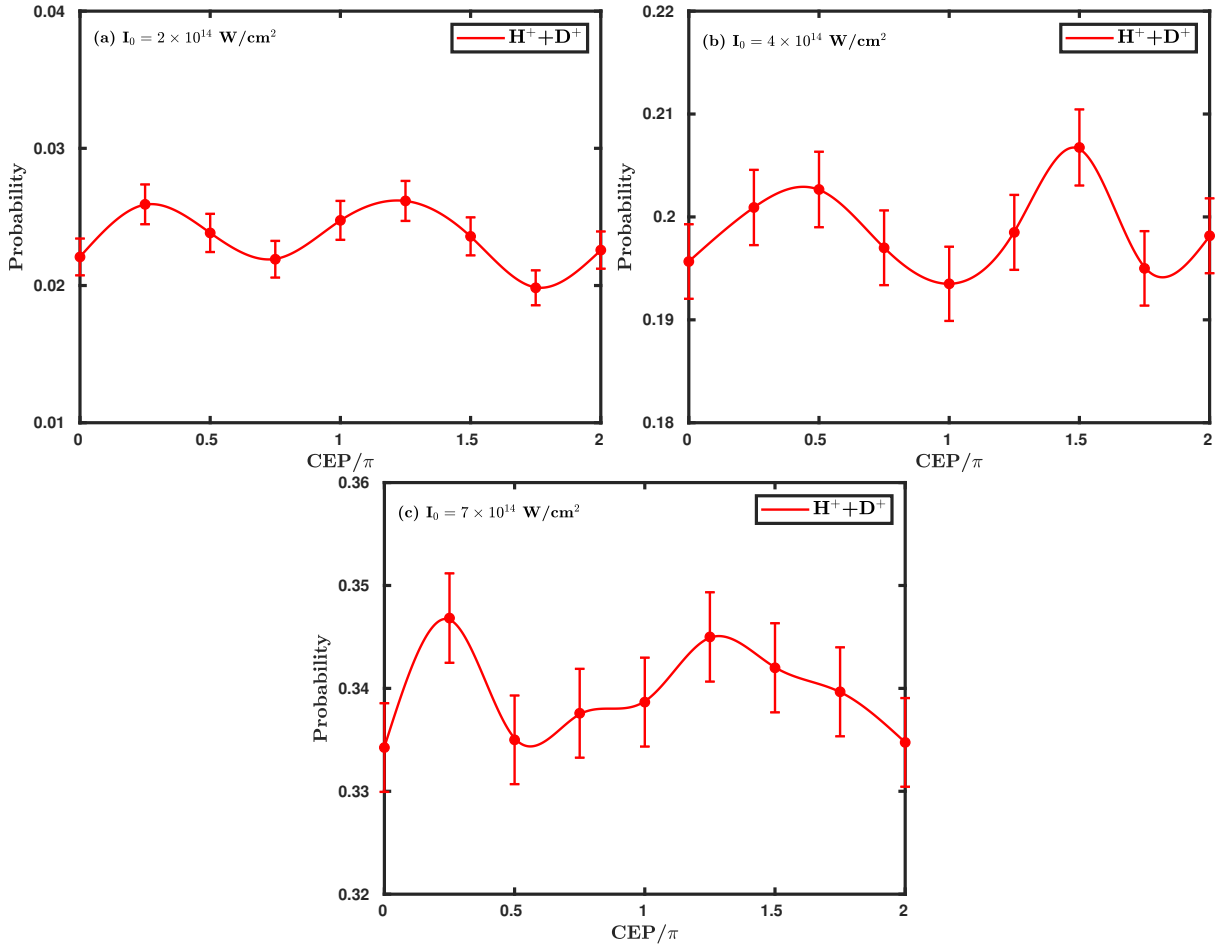

Figure 5: CEP dependence on the Coulomb explosion channel $(H^+ + D^+)$ of HD^+ from the $v = 0$ state. Statistical errors bars are included (see Eq. (5) for details).

with the CEP of the laser pulse. Since the Coulomb explosion probability is minimal at the intensity of 2×10^{14} W/cm^2, so the observed CEP effect on this channel is also less at this

18

intensity. On increasing the laser intensity, the Coulomb explosion probability increases, so the observed CEP effect is also significant at higher intensities. For an intensity of 4×10^{14} W/cm^2, maximum Coulomb explosion probability is found at $\phi = 1.5\pi$ and minimum at $\phi = \pi$, whereas, for intensity 7×10^{14} W/cm^2, the maxima and minima is observed for $\phi = 0.25\pi$ and 0 respectively.

3.4. KER Distributions of the Dissociated Fragments

Another quantity which is sensitive to the CEP of the laser pulses is the KER of the fragments. Fig.6(a) reports the CEP averaged kinetic energy distribution of the H+D$^+$ and D+H$^+$ channels at a peak intensity of 4×10^{14} W/cm^2. The KER of a particular channel is
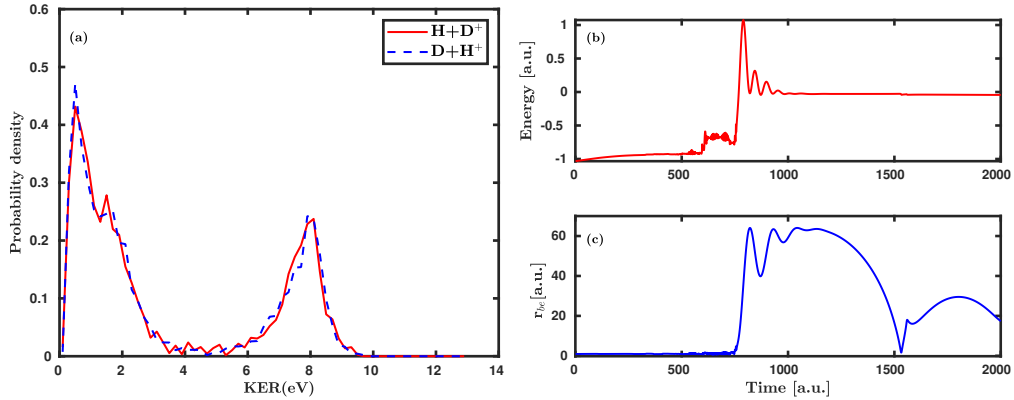

Figure 6: (a) CEP averaged KER distributions for the dissociation channels of HD$^+$ molecular ion with 0.2 eV resolution at an intensity of 4×10^{14} W/cm^2. The errors are in the range of $\pm$ 0.0006, (b) variation of electron energy with time, (c) a particular example of a trajectory indicating the recollision mechanism.

defined as the sum of the kinetic energy of both the nucleus in that channel at the end of the simulation,

$$KER = \frac{p_b^2}{2m_b} + \frac{p_c^2}{2m_c} \tag{6}$$

where p_b and p_c represents the final momentum of the H and D nucleus respectively, m_b and m_c represents the mass of H and D nucleus, respectively. The kinetic energy of the electron

is not included in the definition of KER as we are mainly interested in nuclear kinetic energy spectra. The first peak (at ~ 0.58 eV) mainly arises due to bond softening (BS) dissociation pathway, as suggested in the previous studies.[11,47] Both the channels also consists of another peak (at ~ 8.0 eV) in their KER spectra. Quantum mechanically, this kind of high energy peak is explained by the "frustrated tunneling ionization mechanism" in which one electron first tunneled from the attractive Coulomb potential and then recaptured by the parent atom to form a highly excited neutral atom.[48] As classical mechanics is unable to explain tunneling; therefore, in our classical FMD model, the first step can be understood as over the barrier ionization. For the confirmation of recollision mechanism, we back analyzed the trajectories, which generates such high energy fragments. The temporal evolution of electron energy and the variation of electron-H nucleus distance (r_{be}) for a particular trajectory is shown in fig.6(b) and 6(c), respectively. The electron energy plot indicates the ionization of electron at first, following which, it is recaptured at a later stage. Fig.6(c) shows that at the time of the peak intensity of the laser pulse (at ~ 750 a.u.), electron ejects and decelerates by the electric field then return back to the H-nucleus. This recollision of electron to the nucleus generates the highly excited neutral atom and shows a high energy peak in their KER spectra. It can be inferred from the KER spectra of the dissociation channel that the dissociation does not take place on a single ground state potential. The two peak structure indicates that an excited state is also involved along with the ground state potential; dissociation on the ground state potential results in the low KER fragments, whereas, dissociation on the excited state results in the high KER fragments.

In Fig.6(a), the KER distributions for the $H+D^+$ and $D+H^+$ channels shows almost identical behavior on CEP averaging. To understand the CEP effect on the KER, we evaluated the channel asymmetry parameter (A) defined as
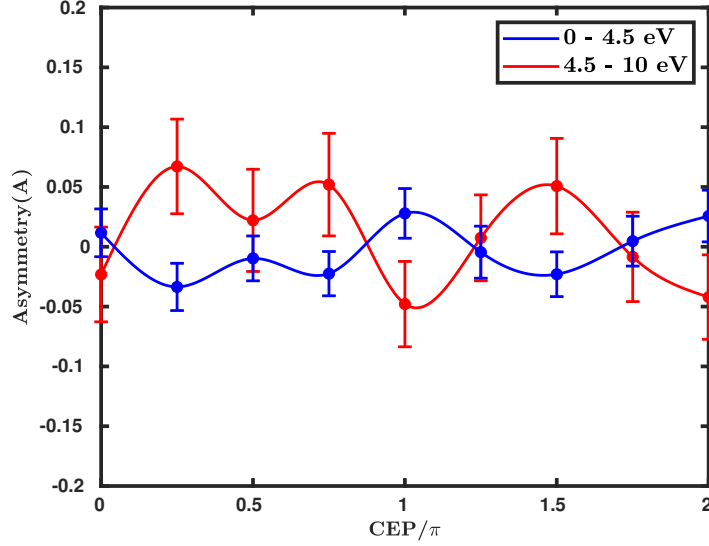
$$A = \frac{P_A - P_B}{P_A + P_B} \tag{7}$$

Figure 7: Channel asymmetry parameter (A) as a function of laser CEP for HD$^+$ ion in presence of 7.1 fs pulse of 4×10^{14} W/cm^2 intensity at two different energy ranges. Statistical errors bars are included (see Eq. (5) for details).

where P_A and P_B are the dissociation yields of H+D$^+$ and D+H$^+$ channels respectively. Fig. 7 reports the asymmetry parameter (A) at some fixed CEP values and for two different KER ranges. This covers the entire kinetic energy range. A clear CEP effect on the dissociation yields of the two channels is noted. For the lower energy range (0 - 4.5 eV), the channel asymmetry parameter (A) shows a relatively smaller variation with the laser CEP compared to the higher energy range (4.5 - 10 eV). For the KER range (4.5 - 10 eV), the D+H$^+$ channel probability is higher than H+D$^+$ channel at CEP values of 0, π, and 2π, whereas, for the rest of the CEP values, H + D$^+$ channel dominates over D + H$^+$ channel. The higher energy fragments (~ 0.8 eV) of the molecular ion are more sensitive to the CEP than the lower energy fragments (~ 0.58 eV). It is clear from Fig.7 that for different energy ranges, the dissociation channel probabilities (H + D$^+$ and D + H$^+$) respond in a different way to the CEP of the laser pulse.

For the ground vibrational state of the molecular ion, the Coulomb explosion channel starts to dominate over the dissociation channel from 4×10^{14} W/cm^2 intensity (see Fig. 2c). Therefore, we calculated the kinetic energy distribution of the fragments in the Coulomb
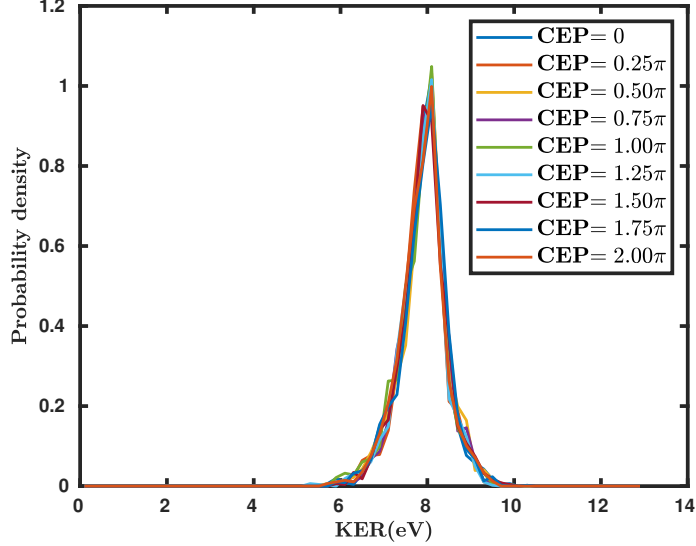
21

Figure 8: KER distribution of the Coulomb explosion channel for HD$^+$ ion with 7.1 fs laser pulse of 4×10^{14} W/cm^2 intensity. The errors are in the range of ± 0.0043.

explosion channel at an intensity of 4×10^{14} W/cm^2, as shown in Fig.8. The KER spectra of HD$^+$ contains only a high energy peak (at ~ 8.0 eV) as expected. The probability of the Coulomb explosion channel is sensitive to the CEP (Fig.5), but in the KER spectra, a notable CEP effect is not found.

A pronounced CEP effect is noted in the probability and KER of the dynamical channels under the influence of 7.1 fs laser pulse as discussed above. In particular, Fig. 4 clearly demonstrates how the dissociation pathways H+D$^+$ and D+H$^+$ can be controlled by varying the laser CEP. Since the CEP controls the waveform of the electric field under the pulse envelope, one expects a larger CEP effect for even shorter laser pulses. Thereby, we repeated our calculations with a shorter pulse (4 fs FWHM) and found an enhanced CEP dependency on the dissociation probability than the 7.1 fs pulse. Fig. 9 shows the variation of dissociation probability of H+D$^+$ and D+H$^+$ with CEP for a 4 fs pulse, starting from the $v = 0$ state of HD$^+$ ion. The difference between the two dissociation channel probabilities for 4 fs pulse is quite significant than for 7.1 fs pulse (see Fig.4d). The maximum difference between the two channels are at CEP values of 0 and 2π. For CEP values of 0, 0.25π and 0.5π, H+D$^+$ channel is larger than D+H$^+$, whereas, for CEP values 0.75π, π and 1.25π, the preference of
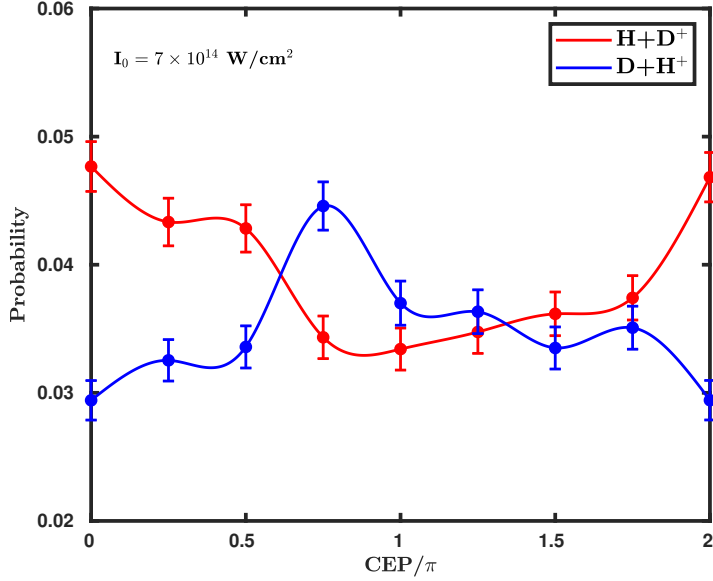
Figure 9: CEP dependence on the dissociation channels of HD^+ ion under 4 fs (790 nm) laser pulse from the $v = 0$ state. Statistical errors bars are included (see Eq. (5) for details).

the channels to dissociate gets reversed. $H+D^+$ channel again starts to dominate over $D+H^+$ channel for CEP values 1.5π, 1.75π, and 2π. Therefore, we can conclude that a larger CEP control of the ultrafast dynamics of HD^+ can be achieved with shorter laser pulses than with larger pulses.

4. Conclusions

In summary, we have theoretically studied the dissociation and ionization dynamics of a randomly oriented HD^+ molecule under ultrashort (7.1 fs) laser pulse (790 nm) with different laser intensities. We employed a well established quasiclassical FMD method to model the dynamics. We reported the temporal evolution of various dynamical channel probabilities and discussed how the molecular ion responds to laser pulse in time. The influence of intensity and initial vibrational states of HD^+ on the dissociation ($H+D^+$ or $D+H^+$) and Coulomb explosion channels ($H^+ + D^+$) for CEP = 0 are reported. At low laser intensities (1×10^{14} and 2×10^{14} W/cm^2), the dissociation channel dominates over the Coulomb explosion

channel, and the dissociation probability increases on increasing the initial vibrational states. At higher intensities (4×10^{14} and 7×10^{14} W/cm^2) Coulomb explosion channel contributes mostly. The CEP effect on the channel probabilities and KER distribution of the dissociation and Coulomb explosion are also investigated. The dissociation and Coulomb explosion probabilities are found to be sensitive to the CEP of the laser pulse. Although the CEP averaged probabilities of H+D$^+$ and D+H$^+$ channels are same, but they differ from each other at fixed CEP values. CEP dependence on different channel probabilities is further affected by the laser field intensity. Therefore, through a careful choice of laser CEP and intensity, one of the channels can be made dominant. The effect of CEP is clearly visible in the channel asymmetry parameter as a function of the KER of fragments. KER spectra of the Coulomb explosion channel is not much affected by the laser CEP. Our results with the FMD model are qualitatively in agreement with the quantum calculation. The difference mainly arises due to our consideration of a randomly oriented molecule in space (with respect to the laser polarization axis), in contrast to an aligned molecule used in the quantum calculation. We also examined how the effect of CEP varies with the pulse width of the laser pulse. CEP effect on the dissociation probabilities for 4 fs pulse is found to be larger than for the 7.1 fs pulse, which again confirms that for shorter pulses the CEP effect is more significant.

This study also confirms that the CEP effect can be explained quasiclassically. In the strong field, the ionized electron is accelerated classically by the laser field. The action accumulated by the electron can reach extremely large value compared to the value of $\hbar$. A large action ensures that we can treat the quantum particles classically.[49] In FMD, there is no restriction on the dimensionality of the system and can be used to simulate the polyatomic molecules in intense laser field. Each trajectory is calculated independently from another, so a large number of trajectories can be easily parallelized by running the trajectories on many processors simultaneously. Moreover, FMD method is a good alternative for the photo-induced dynamical study of polyatomic molecules within certain limitations, e.g., it is

unable to explain quantum mechanical phenomena like diffraction, interference and tunneling which are completely inaccessible to FMD. We believe that our results will stimulate more detailed experiments on the effect of CEP of an ultrashort intense laser pulse on molecular systems.

Acknowledgement

References

(1) Henriksen, N. E. Laser Control of Chemical Reactions. *Chem. Soc. Rev.* **2002**, *31*, 37–42.

(2) Dey, D.; Tiwari, A. K. Coupled Electron–Nuclear Dynamics on H_2^+ within Time-Dependent Born–Oppenheimer Approximation. *J. Phys. Chem. A* **2016**, *120*, 8259–8266.

(3) Cattaneo, L.; Vos, J.; Bello, R. Y.; Palacios, A.; Heuser, S.; Pedrelli, L.; Lucchini, M.; Cirelli, C.; Martín, F.; Keller, U. Attosecond Coupled Electron and Nuclear Dynamics in Dissociative Ionization of H_2. *Nat. Phys.* **2018**, *14*, 733–738.

(4) Gao, W.; Wang, B.-B.; Hu, X.-J.; Chai, S.; Han, Y.-C.; Greenwood, J. Above-Threshold Dissociation of the Molecular Ion HD^+ in a Moderate-Intensity Femtosecond Laser Field from the Calculation of Time-of-Flight Spectra. *Phys. Rev. A* **2017**, *96*, 013426.

(5) Bucksbaum, P. H.; Zavriyev, A.; Muller, H. G.; Schumacher, D. W. Softening of the H_2^+ Molecular Bond in Intense Laser Fields. *Phys. Rev. Lett.* **1990**, *64*, 1883.

(6) Dota, K.; Garg, M.; Tiwari, A.; Dharmadhikari, J.; Dharmadhikari, A.; Mathur, D.

Intense Two-Cycle Laser Pulses Induce Time-dependent Bond Hardening in a Polyatomic Molecule. *Phys. Rev. Lett.* **2012**, *108*, 073602.

(7) Chelkowski, S.; Conjusteau, A.; Zuo, T.; Bandrauk, A. D. Dissociative Ionization of H_2^+ in an Intense Laser Field: Charge-Resonance-Enhanced Ionization, Coulomb Explosion, and Harmonic Generation at 600 nm. *Phys. Rev. A* **1996**, *54*, 3235.

(8) Roudnev, V.; Esry, B. General Theory of Carrier-Envelope Phase Effects. *Phys. Rev. Lett.* **2007**, *99*, 220406.

(9) Paulus, G. G.; Lindner, F.; Walther, H.; Baltuška, A.; Goulielmakis, E.; Lezius, M.; Krausz, F. Measurement of the Phase of Few-Cycle Laser Pulses. *Phys. Rev. Lett.* **2003**, *91*, 253004.

(10) Lindner, F.; Schätzel, M. G.; Walther, H.; Baltuška, A.; Goulielmakis, E.; Krausz, F.; Milošević, D.; Bauer, D.; Becker, W.; Paulus, G. G. Attosecond Double-Slit Experiment. *Phys. Rev. Lett.* **2005**, *95*, 040401.

(11) Kling, M. F.; Siedschlag, C.; Verhoef, A. J.; Khan, J. I.; Schultze, M.; Uphues, T.; Ni, Y.; Uiberacker, M.; Drescher, M.; Krausz, F. et al. Control of Electron Localization in Molecular Dissociation. *Science* **2006**, *312*, 246–248.

(12) Ursrey, D.; Esry, B. Using the Carrier-Envelope Phase to Control Strong-Field Dissociation of HeH$^+$ at Midinfrared Wavelengths. *Phys. Rev. A* **2017**, *96*, 063409.

(13) Li, H.; Kling, N. G.; Förg, B.; Stierle, J.; Kessel, A.; Trushin, S. A.; Kling, M. F.; Kaziannis, S. Carrier-Envelope Phase Dependence of the Directional Fragmentation and Hydrogen Migration in Toluene in Few-Cycle Laser Fields. *Struct. Dyn.* **2016**, *3*, 043206.

(14) Mathur, D.; Dota, K.; Dharmadhikari, A.; Dharmadhikari, J. Carrier-Envelope-Phase

Effects in Ultrafast Strong-Field Ionization Dynamics of Multielectron Systems: Xe and CS$_2$. *Phys. Rev. Lett.* **2013**, *110*, 083602.

(15) Vasa, P.; Dharmadhikari, A. K.; Mathur, D. Carrier-Envelope Phase-Dependent Ionization of Xe in Intense, Ultrafast (two-cycle) Laser Fields. *J. Phys. B: At. Mol. Opt. Phys.* **2017**, *51*, 015601.

(16) Mathur, D.; Dota, K.; Dey, D.; Tiwari, A.; Dharmadhikari, J.; Dharmadhikari, A.; De, S.; Vasa, P. Selective Breaking of Bonds in Water with Intense, 2-Cycle, Infrared Laser Pulses. *J. Chem. Phys.* **2015**, *143*, 244310.

(17) Kato, T.; Yamanouchi, K. Time-Dependent Multiconfiguration Theory for Describing Molecular Dynamics in Diatomic-Like Molecules. *J. Chem. Phys.* **2009**, *131*, 164118.

(18) Lötstedt, E.; Kato, T.; Yamanouchi, K. Time-Dependent Multiconfiguration Method Applied to Laser-Driven H$_2^+$. *Phys. Rev. A* **2019**, *99*, 013404.

(19) Thiele, M.; Gross, E.; Kümmel, S. Adiabatic Approximation in Nonperturbative Time-Dependent Density-Functional Theory. *Phys. Rev. Lett.* **2008**, *100*, 153004.

(20) Heslar, J.; Telnov, D. A.; Chu, S.-I. Time-Dependent Density-Functional Theory with Optimized Effective Potential and Self-Interaction Correction and Derivative Discontinuity for the Treatment of Double Ionization of He and Be Atoms in Intense Laser Fields. *Phys. Rev. A* **2013**, *87*, 052513.

(21) Ho, P. J.; Panfili, R.; Haan, S.; Eberly, J. Nonsequential Double Ionization as a Completely Classical Photoelectric Effect. *Phys. Rev. Lett.* **2005**, *94*, 093002.

(22) Zhou, Y.; Huang, C.; Liao, Q.; Lu, P. Classical Simulations Including Electron Correlations for Sequential Double Ionization. *Phys. Rev. Lett.* **2012**, *109*, 053004.

(23) Kirschbaum, C.; Wilets, L. Classical Many-Body Model for Atomic Collisions Incorporating the Heisenberg and Pauli Principles. *Phys. Rev. A* **1980**, *21*, 834.

(24) Cohen, J. S. Quasiclassical Effective Hamiltonian Structure of Atoms with Z= 1 to 38. *Phys. Rev. A* **1995**, *51*, 266.

(25) LaGattuta, K. Introduction to the Quantum Trajectory Method and to Fermi Molecular Dynamics. *J. Phys. A: Math. Gen.* **2003**, *36*, 6013.

(26) Lötstedt, E.; Midorikawa, K. Ejection of Innershell Electrons Induced by Recollision in a Laser-Driven Carbon Atom. *Phys. Rev. A* **2014**, *90*, 043415.

(27) Lötstedt, E.; Kato, T.; Yamanouchi, K. Classical Dynamics of Laser-Driven D_3^+. *Phys. Rev. Lett.* **2011**, *106*, 203001.

(28) Bauer, D. Small Rare Gas Clusters in Laser Fields: Ionization and Absorption at Long and Short Laser Wavelengths. *J. Phys. B: At. Mol. Opt. Phys.* **2004**, *37*, 3085.

(29) Cohen, J. S. Dissociation and Ionization in Capture of Antiprotons and Negative Muons by the Hydrogen Molecular Ion. *J. Phys. B: At. Mol. Opt. Phys.* **2005**, *38*, 441.

(30) Cohen, J. S. Reactive Collisions of Atomic Antihydrogen with the H_2 and H_2^+ Molecules. *J. Phys. B: At. Mol. Opt. Phys.* **2006**, *39*, 3561.

(31) Frémont, F. Quasiclassical Treatment of the Auger Effect in Slow Ion-Atom Collisions. *Phys. Rev. A* **2017**, *96*, 032712.

(32) Huang, C.; Li, Z.; Zhou, Y.; Tang, Q.; Liao, Q.; Lu, P. Classical Simulations of Electron Emissions from H_2^+ by Circularly Polarized Laser Pulses. *Opt. Express* **2012**, *20*, 11700–11709.

(33) Odenweller, M.; Takemoto, N.; Vredenborg, A.; Cole, K.; Pahl, K.; Titze, J.; Schmidt, L. P. H.; Jahnke, T.; Dörner, R.; Becker, A. Strong Field Electron Emission from Fixed in Space H_2^+ Ions. *Phys. Rev. Lett.* **2011**, *107*, 143004.

(34) Lötstedt, E.; Kato, T.; Yamanouchi, K. D_3^+ and H_3^+ in Intense Laser Fields Studied with a Quasiclassical Model. *Phys. Rev. A* **2012**, *85*, 053410.

(35) Dey, D.; Ray, D.; Tiwari, A. K. Controlling Electron Dynamics with Carrier-Envelope Phases of a Laser Pulse. *J. Phys. Chem. A* **2019**, *123*, 4702–4707.

(36) Paulus, G.; Grasbon, F.; Walther, H.; Villoresi, P.; Nisoli, M.; Stagira, S.; Priori, E.; De Silvestri, S. Absolute-Phase Phenomena in Photoionization with Few-Cycle Laser Pulses. *Nature* **2001**, *414*, 182–184.

(37) Cohen, J. S. Molecular Effects on Antiproton Capture by H_2 and the States of $\overline{pp}$ Formed. *Phys. Rev. A* **1997**, *56*, 3583.

(38) Hijikata, Y.; Nakashima, H.; Nakatsuji, H. Solving Non-Born–Oppenheimer Schrödinger Equation for Hydrogen Molecular Ion and Its Isotopomers Using the Free Complement Method. *J. Chem. Phys.* **2009**, *130*, 024102.

(39) Roudnev, V.; Esry, B. HD^+ in a Short Strong Laser Pulse: Practical Consideration of the Observability of Carrier-Envelope Phase Effects. *Phys. Rev. A* **2007**, *76*, 023403.

(40) Press, W. H.; Flannery, B. P.; Teukolsky, S. A.; Vetterling, W. T. *Numerical Recipes in Fortran 77: The Art of Scientific Computing*; Cambridge University Press, 1992.

(41) LaGattuta, K. Behavior of H_2^+ and H_2 in Strong Laser Fields Simulated by Fermion Molecular Dynamics. *Phys. Rev. A* **2006**, *73*, 043404.

(42) Guo, J.; Liu, X.; Yan, B.; Ding, P. Classical Dynamics of 3D Hydrogen Molecular Ion in Intense Laser Fields. *J. Math. Chem.* **2008**, *43*, 1052–1068.

(43) Pavičić, D.; Kiess, A.; Hänsch, T.; Figger, H. Intense-Laser-Field Ionization of the Hydrogen Molecular Ions H_2^+ and D_2^+ at Critical Internuclear Distances. *Phys. Rev. Lett.* **2005**, *94*, 163002.

(44) Xu, H.; Li, Z.; He, F.; Wang, X.; Atia-Tul-Noor, A.; Kielpinski, D.; Sang, R. T.; Litvinyuk, I. V. Observing Electron Localization in a Dissociating H_2^+ Molecule in Real Time. *Nat. Commun.* **2017**, *8*, 15849.

(45) Rathje, T.; Sayler, A.; Zeng, S.; Wustelt, P.; Figger, H.; Esry, B.; Paulus, G. Coherent Control at Its Most Fundamental: Carrier-Envelope-Phase-Dependent Electron Localization in Photodissociation of a H_2^+ Molecular ion Beam Target. *Phys. Rev. Lett.* **2013**, *111*, 093002.

(46) Dey, D.; Henriksen, N. E. Non-Resonant Vibrational Excitation of HOD and Selective Bond Breaking. *J. Chem. Phys.* **2018**, *148*, 234307.

(47) Sansone, G.; Kelkensberg, F.; Pérez-Torres, J.; Morales, F.; Kling, M. F.; Siu, W.; Ghafur, O.; Johnsson, P.; Swoboda, M.; Benedetti, E. et al. Electron localization following attosecond molecular photoionization. *Nature* **2010**, *465*, 763–766.

(48) Manschwetus, B.; Nubbemeyer, T.; Gorling, K.; Steinmeyer, G.; Eichmann, U.; Rottke, H.; Sandner, W. Strong Laser Field Fragmentation of H_2: Coulomb Explosion without Double Ionization. *Phys. Rev. Lett.* **2009**, *102*, 113002.

(49) Abel, M.; Neumark, D. M.; Leone, S. R.; Pfeifer, T. Classical and Quantum Control of Electrons Using the Carrier-envelope Phase of Strong Laser Fields. *Laser Photon. Rev.* **2011**, *5*, 352–367.

Graphical TOC Entry